

Quasinormal modes, shadow and greybody factors of 5D electrically charged Bardeen black holes

Kimet Jusufi,^{1,2,*} Muhammed Amir,^{3,†} Md Sabir Ali,^{4,‡} and Sunil D. Maharaj^{3,§}

¹*Physics Department, State University of Tetovo,
Ilinden Street nn, 1200, Tetovo, North Macedonia*

²*Institute of Physics, Faculty of Natural Sciences and Mathematics,
Ss. Cyril and Methodius University, Arhimedova 3, 1000 Skopje, North Macedonia*

³*Astrophysics and Cosmology Research Unit, School of Mathematics,
Statistics and Computer Science, University of KwaZulu-Natal,
Private Bag X54001, Durban 4000, South Africa*

⁴*Indian Institute of Technology Ropar, Punjab-140001, India*

(Dated: August 19, 2020)

We study quasinormal modes (QNMs) in 5D electrically charged Bardeen black holes spacetime by considering the scalar and electromagnetic field perturbations. The black holes spacetime is an exact solution of Einstein gravity coupled to nonlinear electrodynamics in five dimensions, which has nonsingular behavior. To calculate QNMs, we use the WKB approximation method up to sixth order. Due to the presence of electric charge $q_e > 0$, both the scalar and electromagnetic field perturbations decay more slowly when compared to the Schwarzschild-Tangherlini black holes. We discover that the scalar field perturbations oscillate more rapidly when compared to the electromagnetic field perturbations. In terms of damping, the scalar field perturbations damp more quickly. Graphically we show that the transmission (reflection) coefficients decrease (increase) with an increase in the magnitude of the electric charge q_e . The emission of gravitational waves allows spacetime to undergo damped oscillations due to the nonzero value of the imaginary part, which is always negative. The imaginary part of the QNMs frequencies is continuously decreasing with an increase in the magnitude of the electric charge q_e for a given mode (l, n) . A connection between the QNMs frequencies and the black hole shadow, as well as the geometric cross-section in the eikonal limit, is also described.

* kimet.jusufi@unite.edu.mk

† amirctp12@gmail.com

‡ sabir.ali@iitrpr.ac.in

§ maharaj@ukzn.ac.za

I. INTRODUCTION

General relativity describes many predictions within its regime and has become the most successful theory of gravity. One of the predictions includes the existence of black holes, as exact solutions to Einstein field equations. Well known black hole spacetimes in general relativity include the exact vacuum/electrovacuum solutions, for example, the Schwarzschild/Reissner-Nordström metric in the static case and the Kerr/Kerr-Newman metric in the stationary axisymmetric case. These solutions contain an unavoidable curvature singularity in their interiors [1]. The Einstein theory of general relativity cannot overcome the existence of singularity in a very high curvature regime. To overcome such singular nature, one could consider regular or nonsingular black holes as possible viable models. Bardeen developed the first model for regular black holes. He studied the collapse of charged matter with a repulsive de Sitter core inside the black hole instead of its singularity [2]. The regularity of the solution means that for a fixed value of the nonlinear parameters, the curvature invariants of the spacetime are finite everywhere, including at the origin, $r = 0$, assuming the limiting curvature condition is satisfied [3]. After its first inception, research on singularity-free models of black holes continued with significant efforts in the last decades. Ayón-Beato and Garcia obtained the first exact spherically symmetric regular black hole solution in which general relativity is coupled to the nonlinear electrodynamics field [4]. In follow up papers, there have been plenty of research work motivated by the idea of regularity. Many exact solutions for regular black holes have been obtained thus far (see [5–10] and references therein). Rotating regular black holes have been a test bed in the non-Kerr family of black holes [11, 12]. They have been used to study several exotic properties ranging from thermal phase transition [13] to shadow properties [14, 15], particle acceleration and particle collisions [16–18], geodesics completeness [19], etc. Regular black hole models have been extended to higher dimensions in modified theories of gravity including Einstein-Gauss-Bonnet [20–23], Lovelock [24], and others [25] to study their various geometrical and physical properties.

Black hole perturbations result in the emission of gravitational waves which are of electromagnetic or scalar nature, characterized by some complex frequencies called the quasinormal modes (QNMs). The real part of the frequencies maintains the oscillations of the gravitational waves while the imaginary part leads to damped or undamped features in its nature. When one detects such waves emanating from the black hole, one could infer relevant information about the particular black hole. The perturbations are needed to extract information about the nature of the astrophysical black holes. Regge and Wheeler [26] performed the first research in this direction and then

Zerilli [27] studied the radial and polar perturbations of the Schwarzschild black holes. They added some small changes onto the unperturbed background, restricting the conditions that the energy-momentum tensor is not affected with such perturbations. Following these works, Vishveshwara [28, 29] and then Chandrasekhar in his monograph [30] explored the QNMs explicitly. The QNMs have been studied for several spacetimes in general relativity as well as in alternative theories of gravity [31–37]. These modes have also been discussed in nonsingular black holes [38, 39]. A study of the QNMs in the context of the AdS/CFT correspondence is also important. It is expected that there may be an exciting correlation between the thermodynamic properties of the loop quantum black holes and the quasinormal ringing of the astrophysical black hole candidates [40, 41]. It may also be valuable to investigate QNMs and a possible connection to the collapsing scenario [42].

A connection between black holes' QNMs and shadows has attracted much attention in recent years as the first image of the black hole was being released. The Event Horizon Telescope group recently detected the black hole images using the shadow properties [43–45]. There exist plenty of work available in the literature on the shadow properties (see [46–56] and references therein). The detection of gravitational waves [57] relating compact objects; such as the black holes are one of the outstanding discoveries which motivate us to study the marriage between the QNMs and the shadow properties of black holes. Therefore, it is very fair and motivating to connect these two properties as they open a new arena in black hole physics. The QNMs and the greybody factors are two important physical phenomena occurring in the curved spacetime background. Furthermore, Hawking radiation is a quantum mechanical effect experienced in curved spacetimes has paramount importance in the study of black holes related phenomena. Particles emitted from the black holes face an effective potential barrier which forces the particles to go back into the black hole; a phenomenon called back-scattering [58]. The greybody factor is a frequency-dependent quantity that measures the deviation from the ideal black body radiation and provides us valuable information about the horizon structure and related physics [59].

The main motivation of this work is to study QNMs frequencies and their connections to the black hole shadow in the 5D electrically charged Bardeen spacetime [60]. Along with this, we also find a relationship between the QNMs frequencies and the greybody factors. Recently, the study connecting the real part of the QNMs frequencies and the shadow radius has been explored in the static spacetime [61, 62] and in the rotating spacetime [63]. Therefore, the discussion of the present work is twofold. On the one hand, we find the QNMs frequencies and on utilizing them, we compute the greybody factors of the black holes. On the other hand, by using the eikonal approximation, we develop a relationship between the QNMs frequencies and the shadow radius of the black holes.

The electrically charged solutions are quite important when discussing regular black hole solutions. The no-go theorem states that there is no Lagrangian function having a Maxwell weak field limit, which gives a solution having a regular center. To evade the no-go theorem, the Einstein gravity must be coupled to nonlinear electrodynamics with a Lagrangian having a proper Maxwell weak field limit. Otherwise, it gives a nontrivial symmetric solution with a globally regular spacetime with the proviso that the electric charge is zero [64–67]. In our Lagrangian, we cannot get the Maxwell limit anywhere, but we are allowed to have regular black holes which are electrically charged as permitted by the no-go theorem. To investigate the stability of the higher dimensional black hole solutions which could exist in nature, we need to derive the spectra of the gravitational QNMs. The damped and undamped situations are related, respectively, to the stable and unstable black holes. The study of the QNMs frequencies have been performed by using many numerical techniques including the WKB method [68], Frobenius method [41], method of continued fractions [69], the Mashhoon method [70, 71], etc. In our work, we follow the WKB approximation method to calculate the QNMs frequencies initially developed by the Schutz and Will [68]. Iyer and Will [72], in their original paper calculated the QNMs up to third order. The higher order contribution was due to Konoplya [40] allowing us to compute the QNMs frequencies without resorting to complicated numerical methods.

The paper is organized as follows. We give a short description of 5D electrically charged Bardeen black holes in Sec. II. The QNMs of black holes are comprehensively discussed in Sec. III. The scattering phenomena and greybody factors are the subject of Sec. IV. Section V is devoted to developing a connection between the QNMs frequencies and the shadow radius, and the absorption cross-section is discussed in VI. We end the paper by concluding the key results in Sec. VII.

II. 5D ELECTRICALLY CHARGED BARDEEN BLACK HOLES

We begin with a brief description of 5D electrically charged Bardeen black holes. The corresponding Einstein-Hilbert action coupled to nonlinear electrodynamics can be expressed [60] as follows

$$S = \frac{1}{16\pi} \int d^5x \sqrt{-g} [R - 4\mathcal{L}(\mathcal{F})], \quad (1)$$

where g represents determinant of the spacetime metric, R is the Ricci scalar, and $\mathcal{L}(\mathcal{F})$ is the Lagrangian of the matter field. Note that the Lagrangian $\mathcal{L}(\mathcal{F})$ is a nonlinear function of the electromagnetic field strength $\mathcal{F} = F_{\mu\nu}F^{\mu\nu}/4$ with $F_{\mu\nu} = \partial_\mu A_\nu - \partial_\nu A_\mu$. By varying the action

with respect to $g_{\mu\nu}$ and A_μ , one could derive the Einstein field equations and the Maxwell equations, respectively. These equations can have the following forms

$$\begin{aligned} R_{\mu\nu} - \frac{1}{2}g_{\mu\nu}R &= 2(\mathcal{L}_{\mathcal{F}}F_{\mu\alpha}F_{\nu}^{\alpha} - g_{\mu\nu}\mathcal{L}), \\ \nabla_{\mu}(\mathcal{L}_{\mathcal{F}}F^{\mu\nu}) &= 0, \end{aligned} \quad (2)$$

where $\mathcal{L}_{\mathcal{F}} = \partial\mathcal{L}/\partial\mathcal{F}$. The nonlinear electrodynamics sources which describe 5D electrically charged Bardeen black holes can be given [60] by the following functions

$$\mathcal{L}(r) = \frac{\mu q_e^3(3q_e^3 - 4r^3)}{(r^3 + q_e^3)^{10/3}}, \quad \mathcal{L}_{\mathcal{F}}(r) = \frac{(r^3 + q_e^3)^{10/3}}{7\mu q_e r^9}. \quad (3)$$

It is noticeable that these nonlinear electrodynamics sources are expressed as a function of r . The corresponding gauge potential is given [60] by

$$A^\mu = -\frac{\mu r^7}{q_e(r^3 + q_e^3)^{7/3}}\delta_t^\mu, \quad (4)$$

and the field strength of the electromagnetic tensor has the form [60] as follows

$$\mathcal{F} = -\frac{49\mu^2 q_e^4 r^{12}}{2(r^3 + q_e^3)^{20/3}}. \quad (5)$$

Thus, the spherically symmetric 5D electrically charged Bardeen black holes spacetime [60] reads simply

$$\begin{aligned} ds^2 &= -f(r) dt^2 + f(r)^{-1} dr^2 \\ &+ r^2 (d\theta^2 + \sin^2\theta d\phi^2 + \cos^2\theta d\psi^2), \end{aligned} \quad (6)$$

where the metric function $f(r)$ has the form

$$f(r) = 1 - \frac{\mu r^2}{(r^3 + q_e^3)^{4/3}}. \quad (7)$$

The parameter q_e represents the nonlinear electric charge and μ is the mass of black holes. The spacetime (6) is asymptotically flat and it does not contain any spacetime singularity, which could be confirmed by computing the curvature scalars [60]. In other words, we can say that the spacetime (6) represents the regular black holes having two horizons, but there is no curvature singularity. Our next task is to compute the quasinormal modes (QNMs) frequencies of the electrically charged Bardeen spacetime.

III. QNMS OF 5D ELECTRICALLY CHARGED BARDEEN BLACK HOLES

In this section, we are going to study the QNMs in 5D electrically charged Bardeen black holes spacetime. QNMs are the solutions of the Schrödinger-like wave equations that satisfy the boundary conditions at the event horizon of black hole and far away from it. We compute the black holes' QNMs frequencies by considering the scalar field perturbations and the electromagnetic field perturbations.

A. Scalar field perturbations

Here we discuss the QNMs of black holes due to the scalar field perturbations. We require a solution to the wave equation in order to compute the QNMs frequencies. Let us start with equation of motion for a massless scalar field which is the Klein-Gordon equation [73], and in background of the curved spacetime can be written as follows

$$\frac{1}{\sqrt{-g}} \partial_\mu (\sqrt{-g} g^{\mu\nu} \partial_\nu \Phi) = 0. \quad (8)$$

Here Φ represents the massless scalar field and it is a function of coordinates $(t, r, \theta, \phi, \psi)$. We further consider an ansatz of the scalar field

$$\Phi(t, r, \theta, \phi, \psi) = \sum_{lm} e^{-i\omega t} \frac{\Psi_l(r)}{r^{3/2}} Y_{lm}(r, \theta), \quad (9)$$

where $e^{-i\omega t}$ represents the time evolution of field and $Y_{lm}(r, \theta)$ denotes the spherical harmonics function. Plunging the ansatz (9) into (8) and applying the separation of variables method, we obtain the standard Schrödinger-like wave equations

$$\frac{d^2 \Psi_l(r_*)}{dr_*^2} + (\omega^2 - V_s(r_*)) \Psi_l(r_*) = 0, \quad (10)$$

where ω is the frequency of perturbation and r_* represents the tortoise coordinates having the relation

$$dr_* = \frac{dr}{f(r)} \Rightarrow r_* = \int \frac{dr}{f(r)}. \quad (11)$$

The advantage of using the tortoise coordinates here is to extend the range used in a survey of the QNMs. The tortoise coordinate is being mapped the semi-infinite region from the horizon to infinity into $(-\infty, +\infty)$ region. The effective potential in (10) takes [74] the following form

$$V_s(r_*) = \left(1 - \frac{\mu r^2}{(r^3 + q_e^3)^{4/3}} \right) \left[\frac{l(l+2)}{r^2} - \frac{6\mu q_e^3 r^2}{(r^3 + q_e^3)^{7/3}} \right] + \frac{3}{4r^2} \left(1 - \frac{\mu r^2}{(r^3 + q_e^3)^{4/3}} \right), \quad (12)$$

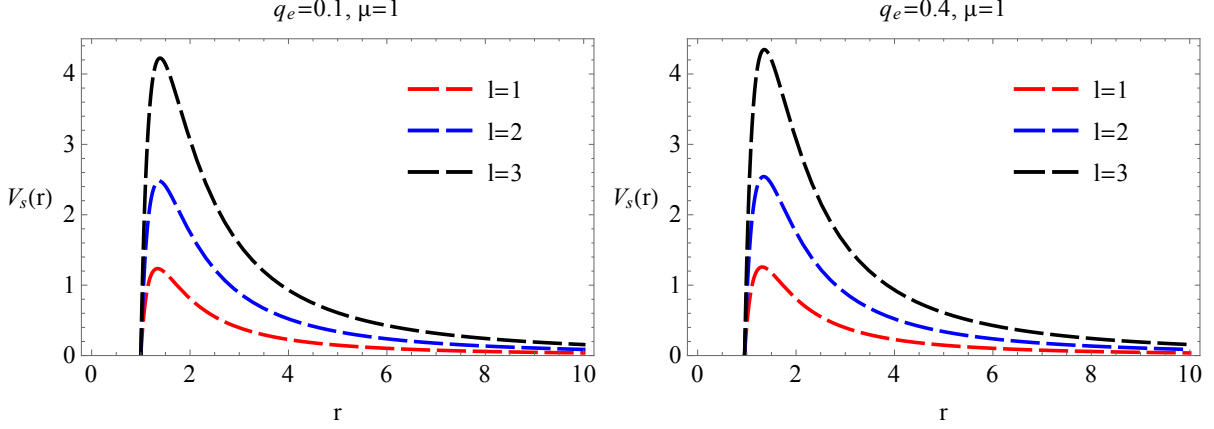


FIG. 1. Plot showing the behavior of effective potential function in case of the scalar field perturbations for different values of multipole number l and electric charge q_e .

where l denotes the multipole number. It is noticeable that the effective potential (12) has the form of a potential barrier. The typical behavior of the effective potential (12) in case of the scalar field perturbations can be seen in Fig. 1 for different values of electric charge q_e and multipole number l .

On having the expression of the effective potential in our hand, we are now in a position to apply the WKB approach in order to compute the QNMs due to the scalar field perturbations. The third order QNMs frequencies are given [72] by

$$\omega^2 = \left(V_0 + \sqrt{-2V_0''} \Lambda_2 \right) - i \left(n + \frac{1}{2} \right) \sqrt{-2V_0''} (1 + \Lambda_3), \quad (13)$$

where Λ_2 and Λ_3 are defined as follows

$$\begin{aligned} \Lambda_2 &= \frac{1}{\sqrt{-2V_0''}} \left[\frac{1}{8} \left(\frac{V_0^{(4)}}{V_0''} \right) \left(\frac{1}{4} + \alpha^2 \right) - \frac{1}{288} \left(\frac{V_0^{(3)}}{V_0''} \right)^2 (7 + 60\alpha^2) \right], \\ \Lambda_3 &= \frac{1}{\sqrt{-2V_0''}} \left[\frac{5}{6912} \left(\frac{V_0^{(3)}}{V_0''} \right)^4 (77 + 188\alpha^2) \right. \\ &\quad - \frac{1}{384} \left(\frac{V_0''' V_0^{(4)}}{V_0''^3} \right) (51 + 100\alpha^2) + \frac{1}{2304} \left(\frac{V_0^{(4)}}{V_0''} \right)^2 (67 + 68\alpha^2) \\ &\quad \left. - \frac{1}{288} \left(\frac{V_0''' V_0^{(5)}}{V_0''^2} \right) (19 + 28\alpha^2) - \frac{1}{288} \left(\frac{V_0^{(6)}}{V_0''} \right) (5 + 4\alpha^2) \right]. \end{aligned} \quad (14)$$

On the other hand, α and $V_0^{(m)}$ have the following definitions

$$\alpha = n + \frac{1}{2}, \quad V_0^{(m)} = \left. \frac{d^m V}{dr_*^m} \right|_{r_*}, \quad (15)$$

where n represents the overtone number. In our study, we are going to consider the sixth order WKB method which is described in [40]. The corresponding formula has the form as follows

$$i \frac{\omega_n^2 - V_0}{\sqrt{-2V_0''}} - \sum_{i=2}^6 \Lambda_i = n + \frac{1}{2}, \quad (16)$$

where the definitions of higher order corrections Λ_4 , Λ_5 , Λ_6 can be found in [40]. Here V_0 represents the height of the barrier and V_0'' denotes the second derivative with respect to the tortoise coordinate of the potential at maximum. Note that all the higher order corrections depend on value of the potential barrier and its higher derivatives at the maximum. Furthermore, we portrait the QNMs frequencies against the electric charge q_e , which can be seen in Figs. 2 and 3. We show various cases of the QNMs frequencies by considering the different values of multipole number l and overtone number n (cf. Figs. 2 and 3). Also, we present the numerical results of the QNMs frequencies in

TABLE I. Real and imaginary parts of the QNMs frequencies in scalar field perturbations ($\mu = 1$).

	$l = 1, n = 0$	$l = 2, n = 0$	$l = 2, n = 1$
q_e	$\omega (WKB)$	$\omega (WKB)$	$\omega (WKB)$
0	1.01444 - 0.36524 i	1.51050 - 0.35770 i	1.39249 - 1.10537 i
0.1	1.01469 - 0.36512 i	1.51087 - 0.35756 i	1.39307 - 1.10491 i
0.2	1.01641 - 0.36426 i	1.51346 - 0.35656 i	1.39717 - 1.10165 i
0.3	1.02126 - 0.36167 i	1.52062 - 0.35371 i	1.40836 - 1.09229 i
0.4	1.03129 - 0.35551 i	1.53516 - 0.34755 i	1.43036 - 1.07169 i
0.5	1.04892 - 0.34209 i	1.56114 - 0.33511 i	1.46649 - 1.02934 i

Table I. We see an increase in the real part of the QNMs frequencies with increasing magnitude of the electric charge q_e (cf. Table I). On the other hand, we find that an increase in the electric charge q_e decreases the imaginary part of the QNMs frequencies in absolute value (cf. Table I). This indicates that the scalar field perturbations in presence of the electric charge $q_e > 0$ decay more slowly compared to the Schwarzschild-Tangherlini black holes. It is worth noting that we have not calculated the QNMs frequencies in case of fundamental mode $l = n = 0$ in Table I. This is related to the fact that the WKB method is applicable when $l > n$ and does not give a satisfactory degree of precision for this fundamental mode ($l = n = 0$). Nevertheless, one can apply other methods for example the Frobenius method to include this fundamental mode (see for example [75]).

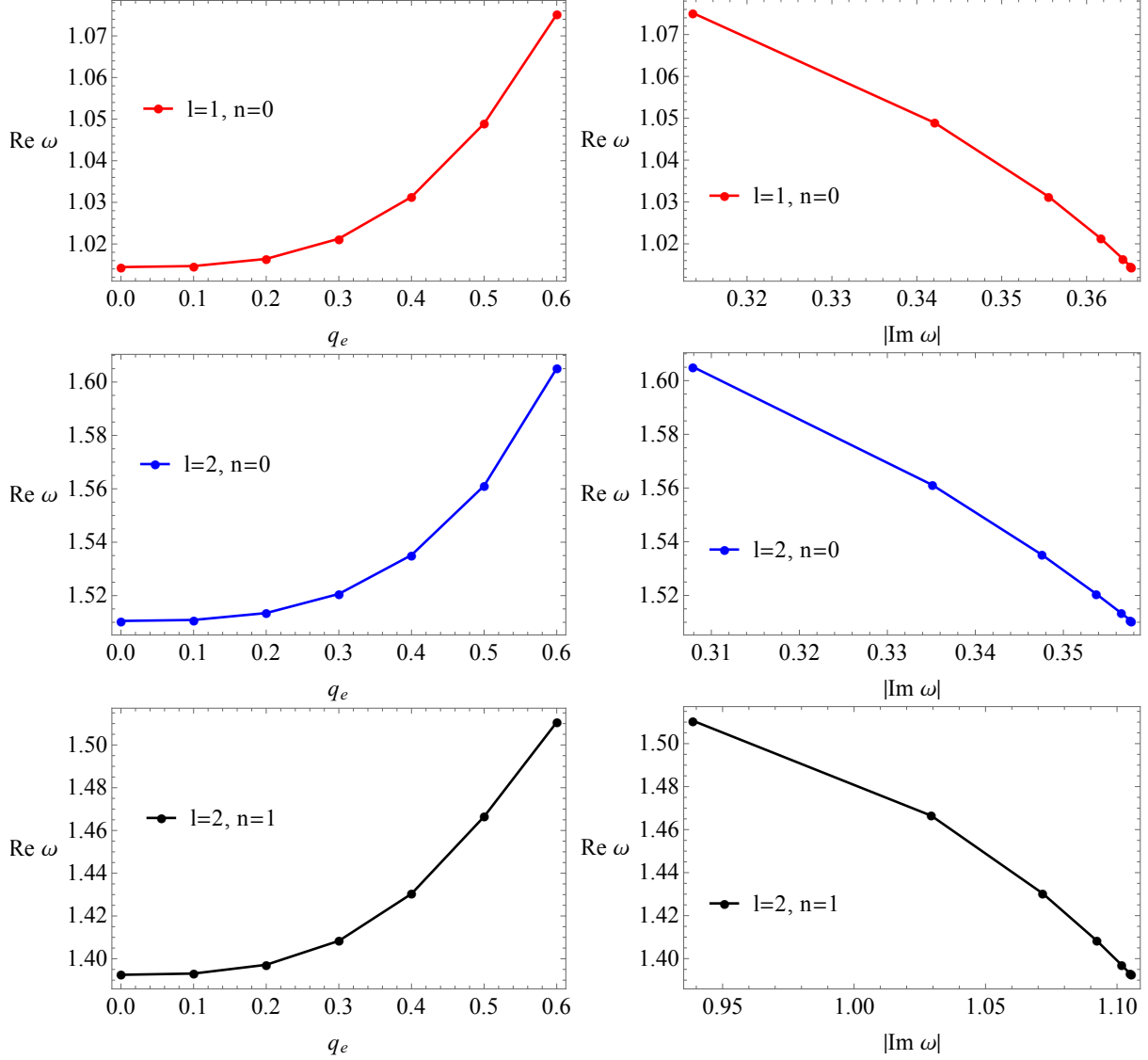


FIG. 2. (Left panel) Plots showing the dependence of real part of the QNMs with electric charge q_e for the scalar field perturbations. (Right panel) Plots showing the dependence of real part of the QNMs versus the imaginary part of the QNMs in absolute value ($\mu = 1$).

B. Electromagnetic field perturbations

In this subsection, we study the QNMs of the black holes by considering the electromagnetic field perturbations. To do so we begin with rewriting the Maxwell equations, $\nabla_\mu(\mathcal{L}_{\mathcal{F}}F^{\mu\nu}) = 0$ as follows

$$\frac{1}{\sqrt{-g}}\partial_\mu \left[\sqrt{-g} \mathcal{L}_{\mathcal{F}} g^{\lambda\mu} g^{\sigma\nu} (\partial_\lambda A_\sigma - \partial_\sigma A_\lambda) \right] = 0. \quad (17)$$

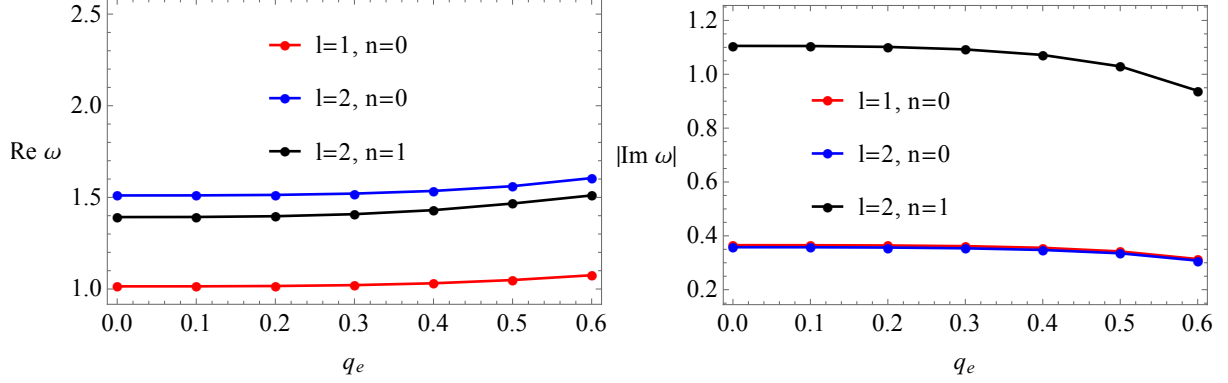


FIG. 3. (Left panel) Plot showing the dependence of real part of the QNMs with electric charge q_e for different values of l and n for the scalar field perturbations. (Right panel) Plot showing the dependence of imaginary part of the QNMs in absolute value with electric charge q_e for different values of l and n ($\mu = 1$).

Now we substitute all related expressions into (17) and using the standard tortoise coordinate transformation $dr_* = dr/f(r)$, which turns out to be the second-order differential equations of following form [76, 77]:

$$\frac{d^2\Psi(r_*)}{dr_*^2} + [\omega^2 - V_{1,2}(r_*)] \Psi(r_*) = 0. \quad (18)$$

Interestingly, we have two categories of the effective potential in case of the higher-dimensional black holes while discussing the electromagnetic field perturbations¹: i) the physical modes **I** of the electromagnetic field perturbations and ii) the physical modes **II** of the electromagnetic field perturbations. Thus, the effective potential corresponding to the modes **I** of the electromagnetic perturbations is given [76, 77] by

$$V_1(r) = \left(1 - \frac{\mu r^2}{(r^3 + q_e^3)^{4/3}}\right) \left[\frac{l(l+2)}{r^2} + \frac{3}{4r^2} \left(1 - \frac{\mu r^2}{(r^3 + q_e^3)^{4/3}}\right) + \frac{2\mu q_e^3 r^2}{(r^3 + q_e^3)^{7/3}}\right], \quad (19)$$

and the effective potential corresponding to the modes **II** of the electromagnetic perturbations has the following form [76, 77]

$$V_2(r) = \left(1 - \frac{\mu r^2}{(r^3 + q_e^3)^{4/3}}\right) \left[\frac{(l+1)^2}{r^2} - \frac{3}{4r^2} \left(1 - \frac{\mu r^2}{(r^3 + q_e^3)^{4/3}}\right) - \frac{2\mu q_e^3 r^2}{(r^3 + q_e^3)^{7/3}}\right]. \quad (20)$$

To see the nature, we illustrate these expressions of the effective potential functions versus radius r . One can see the typical behavior of these effective potentials in Figs. 4 and 5. We find that

¹ Alternatively, one can use the notation of Ref. [78], according to which the physical modes **I** and **II** are noted as scalar type and vector type electromagnetic perturbations, respectively.

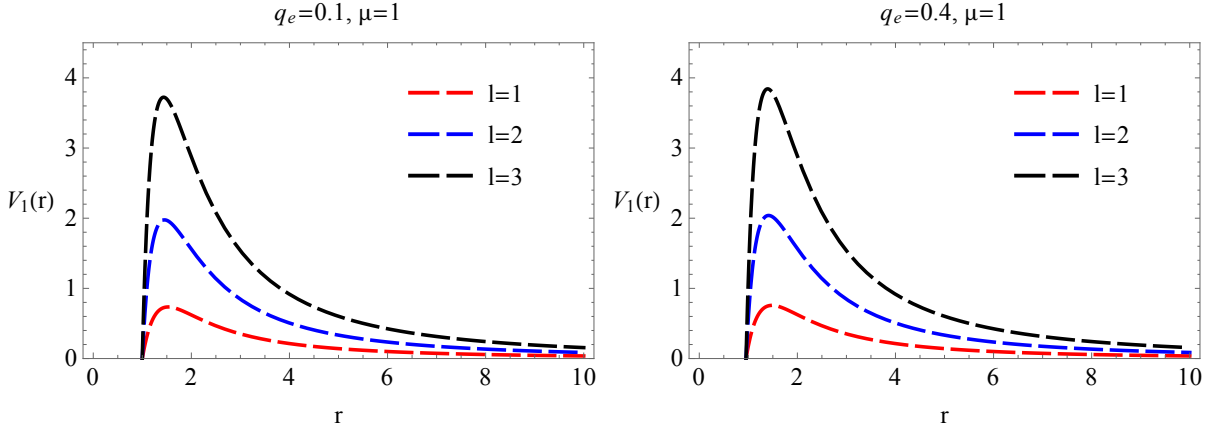


FIG. 4. Plot showing the behavior of effective potential function in the case of modes **I** of the electromagnetic perturbations for different values of multipole number l and electric charge q_e .

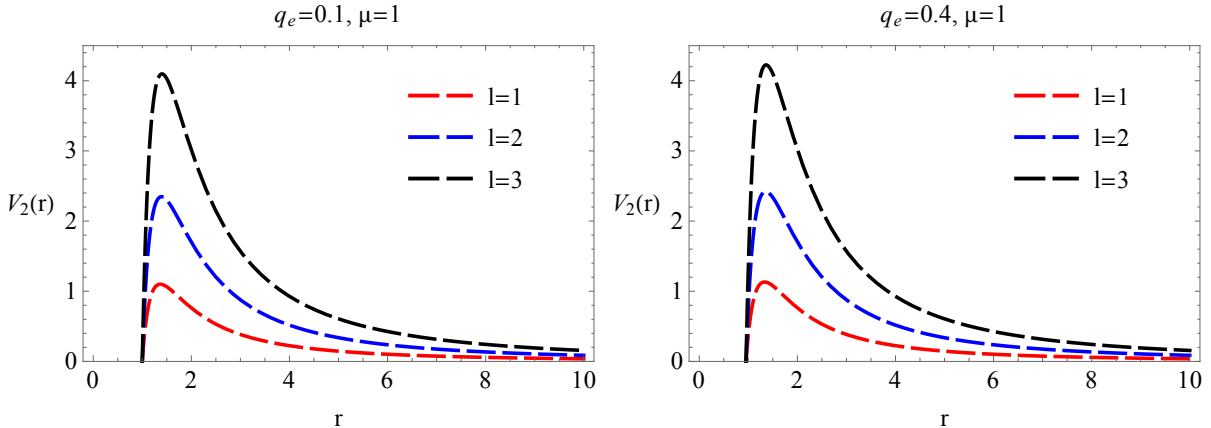


FIG. 5. Plot showing the behavior of effective potential function in the case of modes **II** of the electromagnetic perturbations for different values of multipole number l and electric charge q_e .

an increase in the magnitude of electric charge q_e changes the height of the potential barrier. Similarly, the height of the potential barrier also varies with an increase in multipole number l .

We further present numerical calculations of the QNMs frequencies for the corresponding modes **I** and modes **II** of the electromagnetic field perturbations (cf. Table **II** and **III**). We observe that by increasing the electric charge q_e , the real part of the QNMs frequencies increases while the imaginary part decreases in absolute value compared to the Schwarzschild-Tangherlini black hole. This particular effect can be clearly seen from Figs. **6**, **7**, **8**, and **9**. Moreover, we analyze the numerical results of the real/imaginary part in absolute value of the QNMs frequencies for the corresponding modes **I** and modes **II** of the electromagnetic field perturbations. We find that the modes **II** of the electromagnetic perturbations oscillate and damp more rapidly in comparison to

TABLE II. Real and imaginary parts of the QNMs frequencies in the case of modes **I** of the electromagnetic perturbations ($\mu = 1$).

	$l = 1, n = 0$	$l = 2, n = 0$	$l = 2, n = 1$
q_e	$\omega(WKB)$	$\omega(WKB)$	$\omega(WKB)$
0	0.73685 - 0.31537 i	1.34123 - 0.33725 i	1.21139 - 1.04385 i
0.1	0.73771 - 0.31492 i	1.34165 - 0.33712 i	1.21210 - 1.04342 i
0.2	0.74378 - 0.31183 i	1.34453 - 0.33617 i	1.21702 - 1.04039 i
0.3	0.76020 - 0.30411 i	1.35250 - 0.33352 i	1.23035 - 1.03188 i
0.4	0.79081 - 0.29230 i	1.36856 - 0.32783 i	1.25617 - 1.01378 i
0.5	0.82919 - 0.28502 i	1.39710 - 0.31630 i	1.29788 - 0.97684 i

TABLE III. Real and imaginary parts of the QNMs frequencies in the case of modes **II** of the electromagnetic perturbations ($\mu = 1$).

	$l = 1, n = 0$	$l = 2, n = 0$	$l = 2, n = 1$
q_e	$\omega(WKB)$	$\omega(WKB)$	$\omega(WKB)$
0	0.95143 - 0.35304 i	1.46852 - 0.35248 i	1.34827 - 1.08979 i
0.1	0.95174 - 0.35296 i	1.46894 - 0.35234 i	1.34892 - 1.08934 i
0.2	0.95393 - 0.35240 i	1.47186 - 0.35137 i	1.35348 - 1.08614 i
0.3	0.95996 - 0.35068 i	1.47993 - 0.34858 i	1.36596 - 1.07699 i
0.4	0.97226 - 0.34634 i	1.49638 - 0.34253 i	1.39060 - 1.05692 i
0.5	0.99438 - 0.33563 i	1.52601 - 0.33011 i	1.43181 - 1.01517 i

the modes **I** (cf. Table [II](#) and [III](#)).

Furthermore, we compare the numerical results of the scalar field perturbations and the electromagnetic field perturbations. We find that the numerical values of the real/imaginary part of the QNMs frequencies in absolute value are comparatively higher in the scalar field perturbations (cf. Table [I](#), [II](#) and [III](#)). It turns out that the scalar field perturbations oscillate more rapidly compared to the electromagnetic ones. On the other hand, the scalar field perturbations damp more rapidly than the electromagnetic ones. In general, both the electromagnetic and scalar field perturbations in presence of the electric charge q_e decay more slowly compared to the Schwarzschild-Tangherlini black holes.

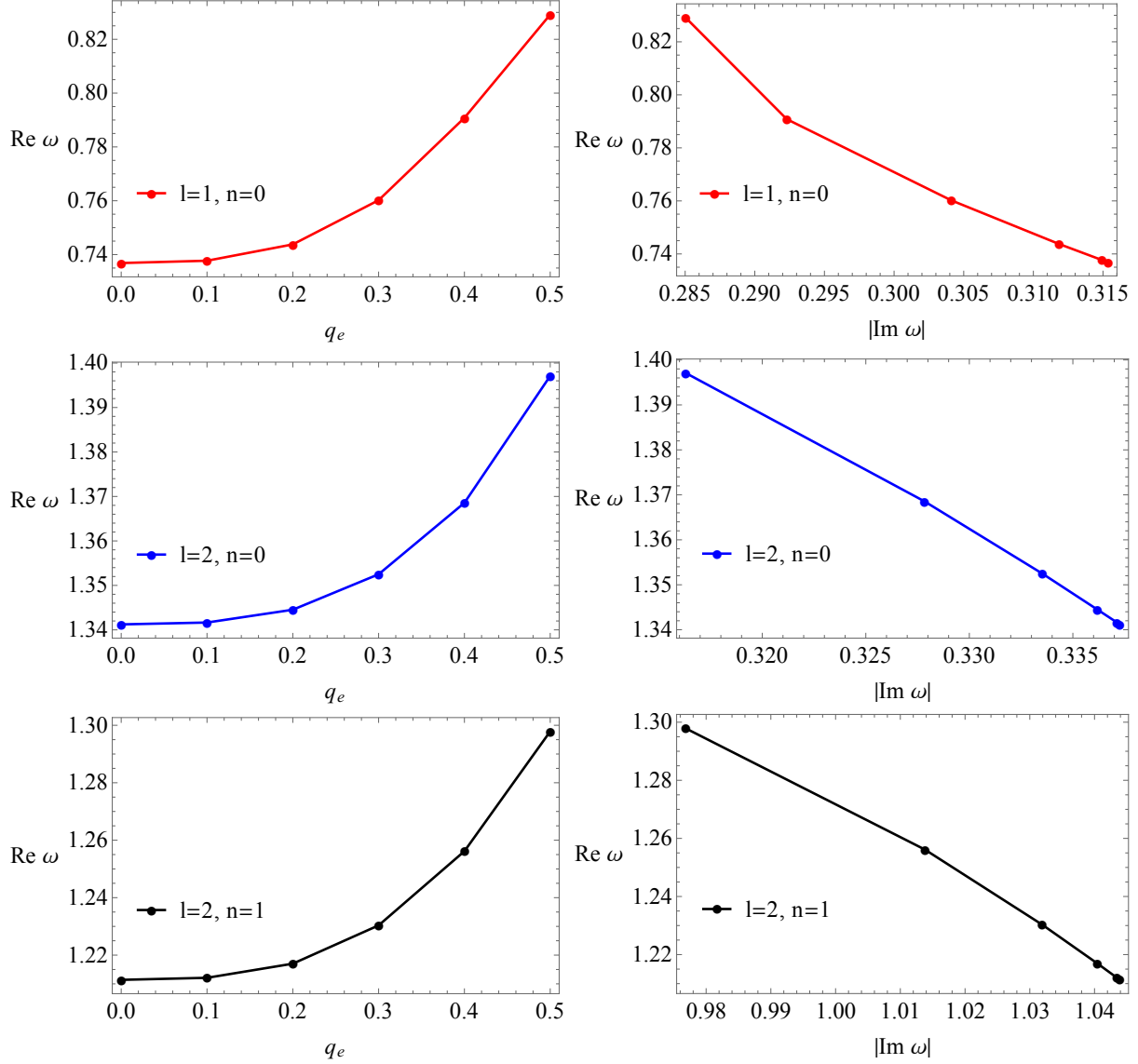


FIG. 6. (Left panel) Plot showing the dependence of real part of the QNMs with electric charge q_e for the modes I of the electromagnetic field perturbations. (Right panel) Plot showing the dependence of real part of the QNMs versus the imaginary part of the QNMs in absolute value ($\mu = 1$).

IV. SCATTERING AND GREYBODY FACTORS

Now we are going to discuss the greybody factors in 5D electrically charged Bardeen black holes spacetime. This study is vital to determine, for instance, the amount of initial quantum radiation in the vicinity of the event horizon of black hole, which is reflected back to it by the potential barrier. Therefore, it is natural to interpret the greybody factors as the tunneling probability of the wave through the barrier determined by the effective potential in given black hole spacetime. We begin

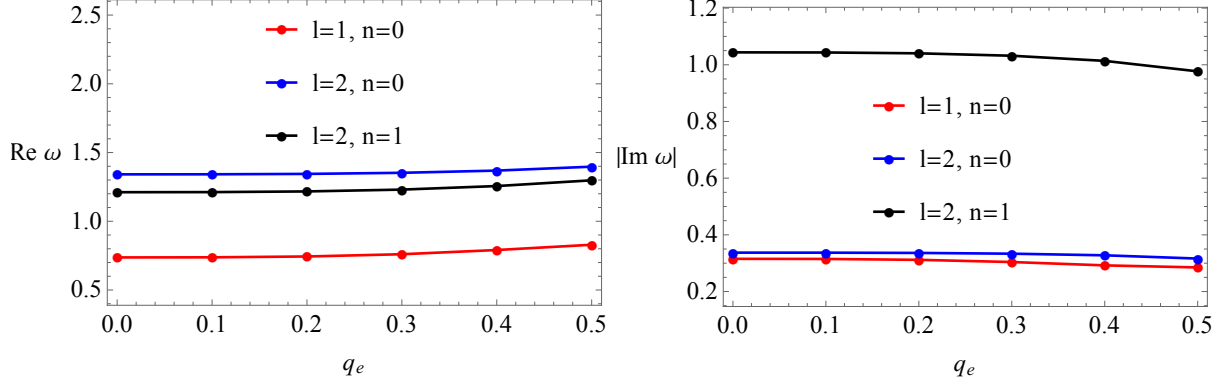


FIG. 7. (Left panel) Plots showing the dependence of real part of the QNMs with electric charge q_e for different values of l and n for the modes **I** of the electromagnetic perturbations. (Right panel) Plots showing the dependence of real part of the QNMs in absolute value with electric charge q_e for different values of l and n ($\mu = 1$).

with the Schrödinger-like equation that describes the scattering of waves in 5D electrically charged Bardeen black hole spacetime. The asymptotic solutions of the Schrödinger-like equation are given as follows

$$\Psi = Ae^{-i\omega r_*} + Be^{i\omega r_*}, \quad r_* \rightarrow -\infty, \quad (21)$$

$$\Psi = Ce^{-i\omega r_*} + De^{i\omega r_*}, \quad r_* \rightarrow +\infty, \quad (22)$$

where A, B, C , and D are functions of the frequency ω . Furthermore, we need to impose the conditions $B(\omega) = 0$, for waves coming to the black hole from infinity and $R(\omega) = D(\omega)/C(\omega)$, for the reflection amplitude. It is worth noting that these waves are identical to that of the scattered ones due to the black holes' event horizon. The transmission amplitude is given by $T(\omega) = A(\omega)/C(\omega)$, thence

$$\Psi = Te^{-i\omega r_*} \quad r_* \rightarrow -\infty, \quad (23)$$

$$\Psi = e^{-i\omega r_*} + Re^{i\omega r_*}, \quad r_* \rightarrow +\infty. \quad (24)$$

Our next task is to determine the square of the wave function's amplitude. To achieve this goal, we can use the fact that the total probability of finding wave must obey the normalization condition given by

$$|R|^2 + |T|^2 = 1. \quad (25)$$

While discussing the greybody factors, we consider the scenario $\omega \simeq V(r_0)$, which is the most

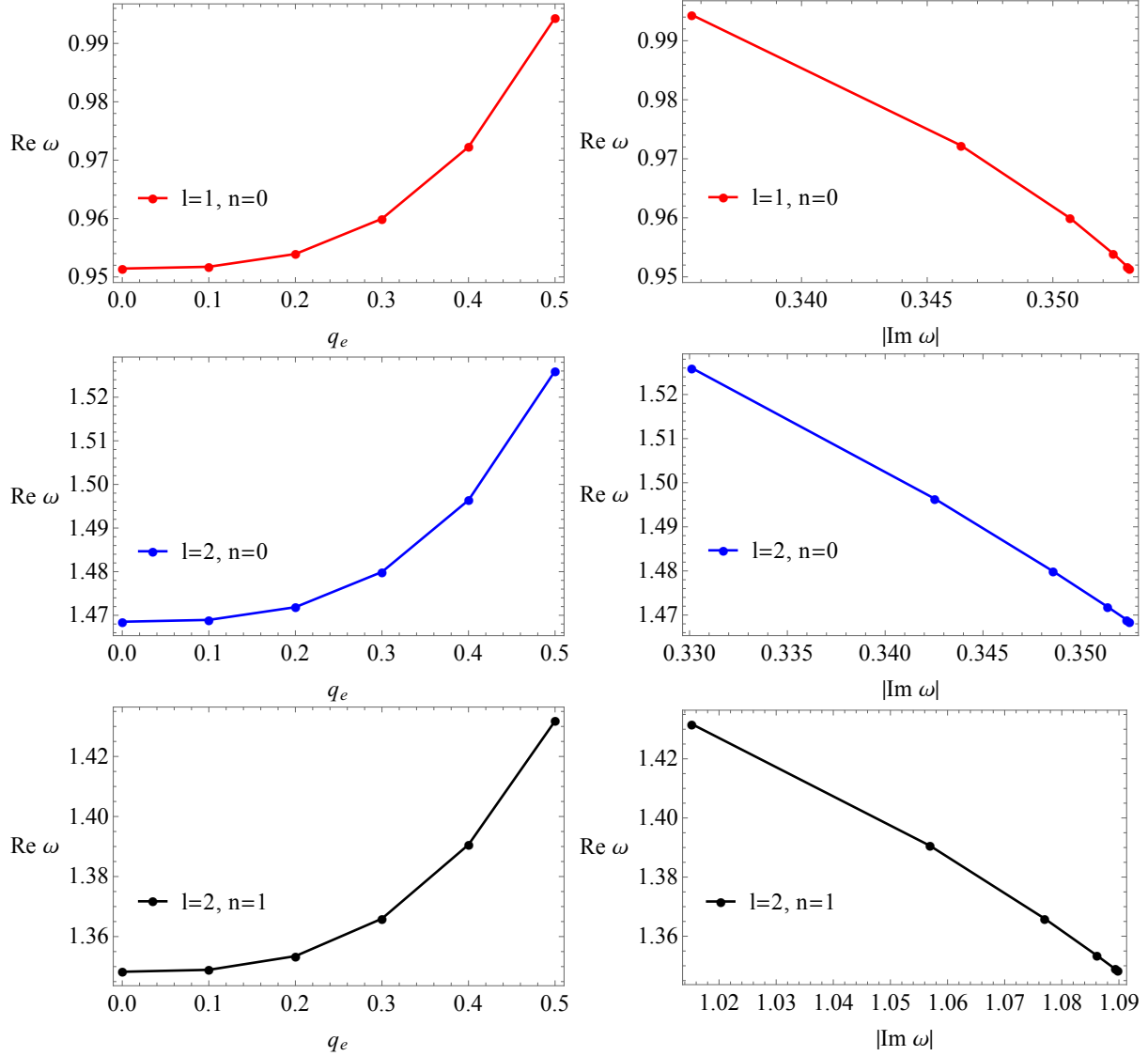


FIG. 8. (Left panel) Plots showing the dependence of real part of the QNMs with electric charge q_e for the modes **II** of the electromagnetic field perturbations. (Right panel) Plots showing the dependence of real part of the QNMs versus the imaginary part of the QNMs in absolute value ($\mu = 1$).

compelling case. Note that, in general, the Schrödinger-like equation cannot be solved analytically. Therefore, to compute the reflection and transmission coefficients, we follow the WKB approximation approach. On using the above equations, it is not difficult to show that the reflection coefficient is given by

$$R = \frac{1}{\sqrt{1 + \exp(-2\pi i K)}}, \quad (26)$$

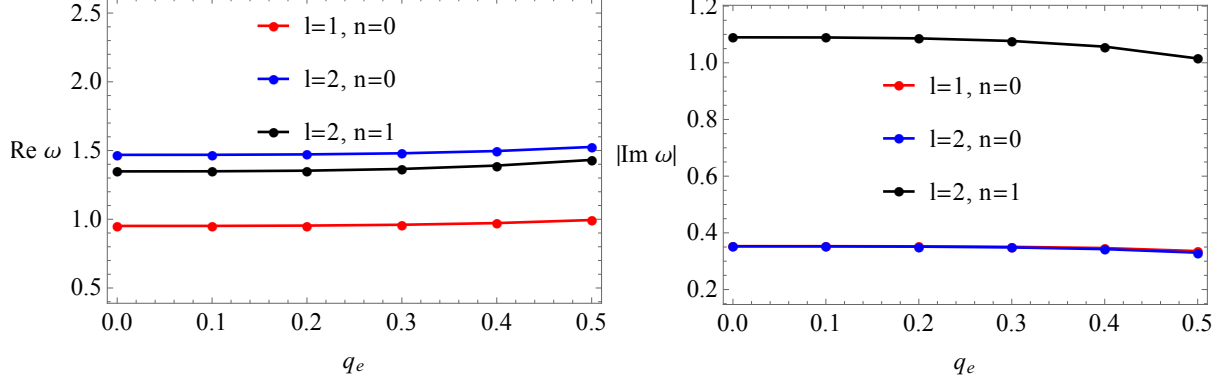


FIG. 9. (Left panel) Plots showing the dependence of real part of the QNMs with electric charge q_e for different values of l and n for the modes **I** of the electromagnetic perturbations. (Right panel) Plots showing the dependence of real part of the QNMs in absolute value with electric charge q_e for different values of l and n ($\mu = 1$).

where K is expressed as follows

$$K = i \frac{\omega_n^2 - V(r_0)}{\sqrt{-2V''(r_0)}} - \sum_{i=2}^6 \Lambda_i. \quad (27)$$

On having the expression of the reflection coefficient, now we can use the condition (25) to obtain the transmission coefficient which takes the following form

$$|T|^2 = 1 - \left| \frac{1}{\sqrt{1 + \exp(-2\pi i K)}} \right|^2. \quad (28)$$

To see the nature of these coefficients, we plot them against frequency ω for different values of the electric charge q_e . The typical behavior of them is illustrated in Fig. 10. We show the effect of the electric charge q_e on the transmission and the reflection coefficients in case of both the scalar and electromagnetic field perturbations (cf. Fig. 10). We find that an increase in the magnitude of electric charge q_e decreases the transmission coefficient in both cases of the perturbations. On the other hand, we observe the opposite effect of electric charge q_e on the reflection coefficient when compared to the transmission coefficient. It turns out that the reflection coefficient increases with increasing magnitude of the electric charge q_e .

V. CONNECTION BETWEEN SHADOW RADIUS AND QNMS

Here we investigate a relationship between the black hole shadow and the real part of QNMs frequencies. To show this correspondence, let us first study the shadow of the 5D electrically

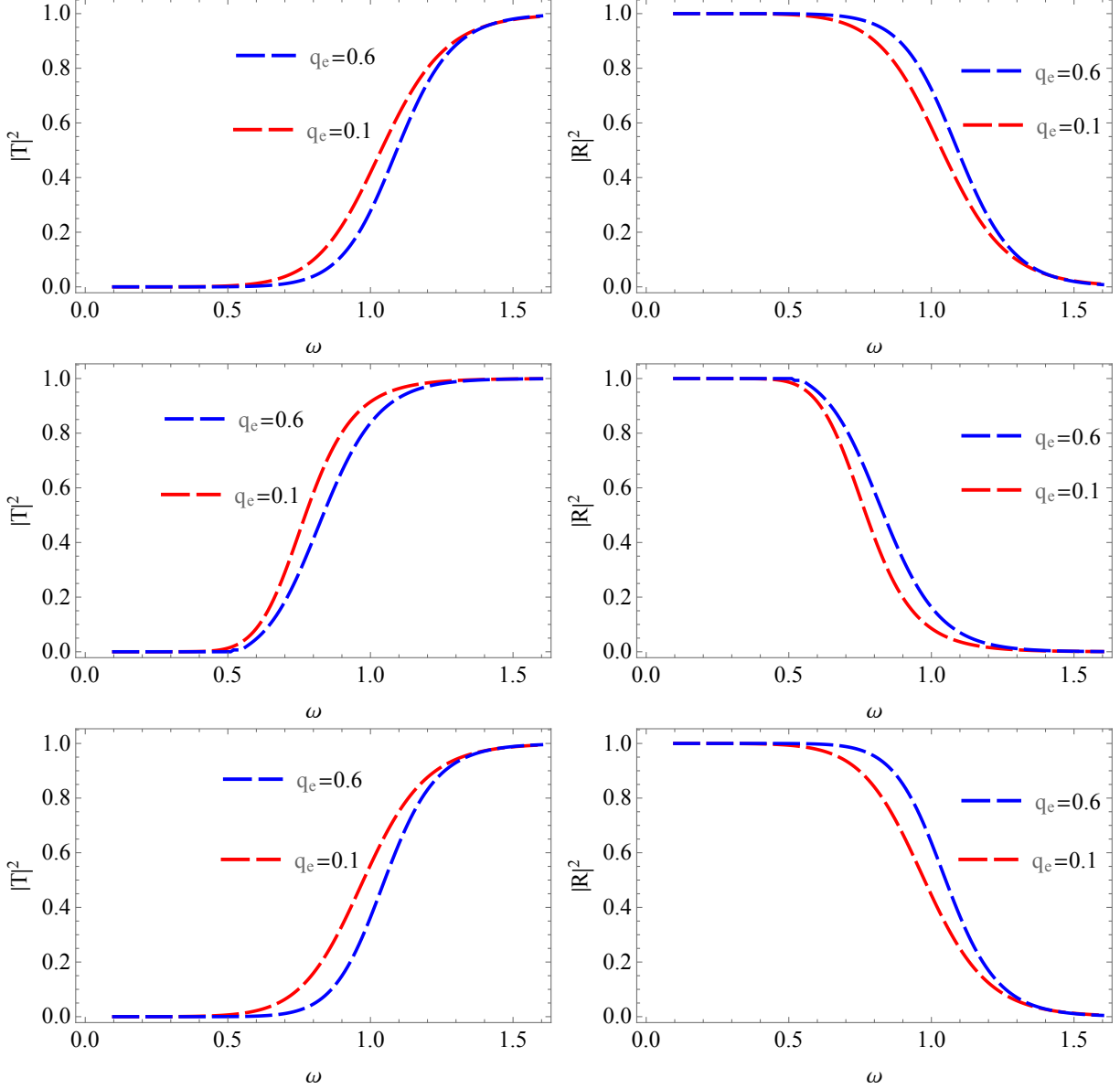


FIG. 10. (Left panel): From top to bottom, plots showing the behavior of transmission coefficients for the scalar field perturbations and electromagnetic field perturbations for the modes **I** and **II**, respectively. (Right panel): From top to bottom, plots showing the reflection coefficient for the scalar field perturbations and electromagnetic field perturbations for the modes **I** and **II**, respectively ($\mu = 1$ and $l = 1$).

charged Bardeen black holes using the geodesic approach. As we know from the symmetry of the spacetime (6), it admits three Killing vectors, namely ∂_t , ∂_ϕ , and ∂_ψ . The presence of these Killing vectors can give rise to the associated conserved quantities, namely, the energy E , and the two angular momenta L_ϕ and L_ψ in ϕ and ψ directions, respectively. By using these conserved

quantities and their relations with conjugate momenta, we can easily have the geodesic equations

$$\begin{aligned}\frac{dt}{d\sigma} &= \frac{E}{f(r)}, \\ \frac{d\phi}{d\sigma} &= \frac{L_\phi}{r^2 \sin^2 \theta}, \\ \frac{d\psi}{d\sigma} &= \frac{L_\psi}{r^2 \cos^2 \theta},\end{aligned}\tag{29}$$

where σ is an affine parameter. Apart from these geodesic equations, the radial and the angular geodesic equations can be derived by using the Hamilton-Jacobi equation

$$\frac{\partial S}{\partial \sigma} = -\frac{1}{2}g^{\mu\nu} \frac{\partial S}{\partial x^\mu} \frac{\partial S}{\partial x^\nu},\tag{30}$$

where S being the Jacobi action. The Jacobi action S can be separated in the following form

$$S = \frac{1}{2}m_0^2\sigma - Et + L_\phi\phi + L_\psi\psi + S_r(r) + S_\theta(\theta),\tag{31}$$

where S_r and S_θ are functions of r and θ only, respectively. The parameter m_0 denotes the mass of the test particle that vanishes in the photon's case. We now substitute (31) into (30), and after some straightforward calculations, we obtain

$$\begin{aligned}r^2 \frac{dr}{d\sigma} &= \pm \sqrt{\mathcal{R}(r)}, \\ r^2 \frac{d\theta}{d\sigma} &= \pm \sqrt{\Theta(\theta)},\end{aligned}\tag{32}$$

where the function $\mathcal{R}(r)$ and $\Theta(\theta)$ reads simply

$$\begin{aligned}\mathcal{R}(r) &= E^2 r^4 - r^2 f(r) (\mathcal{K} + L_\phi^2 + L_\psi^2), \\ \Theta(\theta) &= \mathcal{K} - L_\phi^2 \cot^2 \theta - L_\psi^2 \tan^2 \theta.\end{aligned}\tag{33}$$

Here \mathcal{K} denotes the Carter constant which appears when we separate the coefficients of r and θ during the Hamilton-Jacobi formulation.

In order to describe the black hole shadow, we introduce the celestial coordinates which in case of the 5D black holes are given [79] as following:

$$\begin{aligned}x &= - \lim_{r_0 \rightarrow \infty} r_0 \frac{p^{\hat{\phi}} + p^{\hat{\psi}}}{p^{\hat{t}}}, \\ y &= \lim_{r_0 \rightarrow \infty} r_0 \frac{p^{\hat{\theta}}}{p^{\hat{t}}},\end{aligned}\tag{34}$$

where $p^{\hat{i}}$ being the contravariant components of the momenta in new coordinate basis. These contravariant components of the momenta can be easily computed by using the orthonormal basis vectors for the local observer [79, 80], they become

$$\begin{aligned} p^{\hat{t}} &= \frac{E}{f(r)}, & p^{\hat{\phi}} &= \frac{L_{\phi}}{r \sin \theta}, & p^{\hat{\psi}} &= \frac{L_{\psi}}{r \cos \theta}, \\ p^{\hat{r}} &= \pm \sqrt{f(r)\mathcal{R}(r)}, & p^{\hat{\theta}} &= \pm \frac{\sqrt{\Theta(\theta)}}{r}. \end{aligned} \quad (35)$$

Plunging (35) into (34) and taking the limit $r_0 \rightarrow \infty$, provides

$$\begin{aligned} x &= -(\xi_{\phi} \csc \theta + \xi_{\psi} \sec \theta), \\ y &= \pm \sqrt{\eta - \xi_{\phi}^2 \cot^2 \theta - \xi_{\psi}^2 \tan^2 \theta}, \end{aligned} \quad (36)$$

where we introduce the new quantities, $\xi_{\phi} = L_{\phi}/E$, $\xi_{\psi} = L_{\psi}/E$, and $\eta = \mathcal{K}/E^2$. These quantities are also known as the impact parameters. We now derive the limiting cases of (36) according to the location of the observer. If the observer is situated in equatorial plane ($\theta_0 = \pi/2$), then the angular momentum $L_{\psi} = 0$, which implies $\xi_{\psi} = 0$, thus we have

$$x = -\xi_{\phi}, \quad y = \pm \sqrt{\eta}. \quad (37)$$

On the other hand, when $\theta_0 = 0$, in this case $L_{\phi} = 0$, which implies $\xi_{\phi} = 0$, thereby

$$x = -\xi_{\psi}, \quad y = \pm \sqrt{\eta}. \quad (38)$$

Equations (37) and (38) represent a connection between the celestial coordinates and the impact parameters when the observer is situated at inclination angles $\theta_0 = \pi/2$ and $\theta_0 = 0$, respectively. These equations are crucial to extract the information regarding the shadows of the black holes.

We further derive a relationship between the impact parameters of the spacetime (6) by using the unstable spherical photon orbits conditions, $\mathcal{R} = 0$ and $d\mathcal{R}/dr = 0$, which turns out to be

$$\eta + \xi_{\phi}^2 + \xi_{\psi}^2 = \frac{r^2}{f(r)}, \quad r = \frac{2f(r)}{f'(r)}, \quad (39)$$

where prime (\prime) denotes the derivative with respect to r . Note that the metric function $f(r)$ is defined in (7) and the derivative of it with respect to r reads simply

$$f'(r) = \frac{2\mu(r^4 - q_e^3 r)}{(r^3 + q_e^3)^{7/3}}. \quad (40)$$

On having all the related expressions with us, now we can portrait the shadows of the 5D electrically charged Bardeen black holes. The behavior of the shadows with electric charge q_e can be seen in

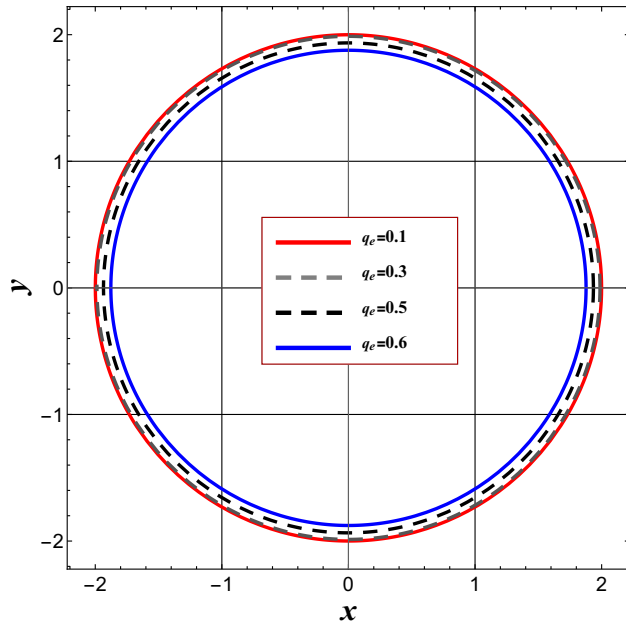


FIG. 11. Illustration of shadows of the 5D electrically charged Bardeen black holes for different values of electric charge q_e ($\mu = 1$).

Fig. 11. We notice that the shape of the black hole shadow is a perfect circle. We see a decrease in radius of the black hole shadow with increasing magnitude of the electric charge q_e . Thus, we can conclude that the electric charge q_e decreases the radius of the black hole shadow.

Now we proceed further to investigate the correspondence between the radius of the black hole shadow and the real part of the QNMs frequency. It has been argued in a seminal paper by Cardoso *et al.* [81] that in the eikonal limit, the real part of the the QNMs frequencies is related to the angular velocity of the unstable null geodesic. However, the imaginary part of the QNMs frequencies is associated to the Lyapunov exponent that determines the instability time scale of the orbits. This can be easily understood by the following equation [81]

$$\omega_{QNM} = \Omega_c l - i \left(n + \frac{1}{2} \right) |\lambda|, \quad (41)$$

where Ω_c is the angular velocity at the unstable null geodesic, and λ denotes the Lyapunov exponent. Furthermore, this correspondence is expected to be valid not only for the static spacetimes but also for the stationary ones. On the other hand, Stefanov *et al.* [82] showed a connection between the QNMs frequencies and the strong gravitational lensing of the spherically symmetric black holes spacetime. Most recently, one of the authors of this paper pointed out that the following relation relates the real part of the QNMs frequencies and the shadow radius (see for details

[61, 83])

$$\omega_{\Re} = \lim_{l \gg 1} \frac{l}{R_s}, \quad (42)$$

which is precise only in the eikonal limit having large values of multipole number l . Here R_s denotes the radius of the black hole shadow. Hence, we can quickly rewrite the expression (41) as follows

$$\omega_{QNM} = \lim_{l \gg 1} \frac{l}{R_s} - i \left(n + \frac{1}{2} \right) |\lambda|. \quad (43)$$

The importance of this correspondence relies on the fact that the shadow radius represents an observable quantity which can be measured by using direct astronomical measurement. Therefore, it is more convenient to express the real part of the QNMs frequencies in terms of the black hole shadow radius instead of the angular velocity. Another advantage of using (42) is the possibility to determine the shadow radius once we have calculated the real part of QNMs and this, in turn, does not necessitate the use of the standard geodesic method. This close connection could be understood from the fact that the gravitational waves can be treated as massless particles propagating along the last null unstable orbit and out to infinity. It is thus expected that, in the eikonal limit, this correspondence could be valid for the scalar, the electromagnetic, and the gravitational field perturbations because they have the same behavior. Surprisingly, the link between the null geodesics and the QNMs frequencies is shown to be violated in the Einstein-Lovelock theory, even in the eikonal limit [84]. We therefore say that the correspondence between the real part of the QNMs frequencies and the shadow radius is not guaranteed for the gravitational field perturbations in the Einstein-Lovelock theory. Although the relation (42) is accurate only for large l , this relation can provide valuable information regarding the effect of the electric charge q_e on the shadow radius even for small l . We can illustrate this fact using the numerical results of the real part of the QNMs frequencies presented in Tables I, II and III, respectively. As we have already seen that the real part of the QNMs frequencies ω_{\Re} increases with the electric charge q_e . Therefore, if we use the inverse relationship between ω_{\Re} and the shadow radius R_S ,

$$\omega_{\Re}(q_e) \propto \frac{1}{R_s(q_e)}, \quad (44)$$

it follows that the shadow radius should decrease by increasing the magnitude of the electric charge q_e . This effect indeed is shown to be the case as depicted in Fig. 11 by using the geodesic method. It is quite surprising that we can deduce this information directly from the inverse relationship between the real part of the QNMs frequencies and the shadow radius (42), even in case of the small multipole number l . However, the relation (42) is precise only in the eikonal regime having

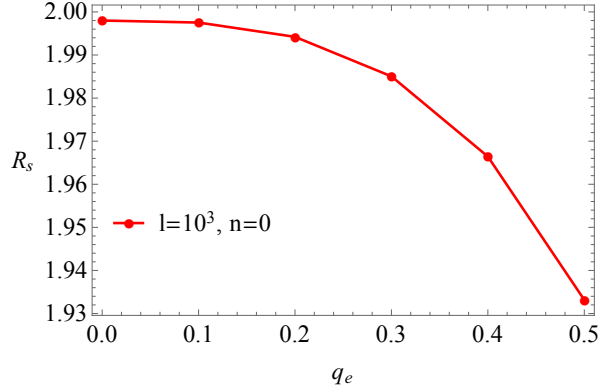


FIG. 12. Shadow radius of the 5D electrically charged Bardeen black holes as a function of electric charge q_e obtained via the relation (42) with mass $\mu = 1$.

$l \gg 1$. We use relation (42) to demonstrate the effect of electric charge q_e on the shadow radius (cf. Fig. 12). We also discover that the shadow radius of the 5D electrically charged Bardeen black holes is smaller than that of the 5D Schwarzschild-Tangherlini black holes. On the other hand, sometimes we use the inverse setup; namely, we can evaluate numerically the shadow radius R_s from the geodesic equations to find the real part of QNMs frequencies. To illustrate this fact, we use the correspondence between the shadow radius of black hole and the real part of QNMs frequencies to the sub-leading regime to half of its value for the D -dimensional case reported recently in [62]:

$$\omega_{\Re} = R_s^{-1} \left(l + \frac{D-3}{2} \right). \quad (45)$$

It is clear from (45) that in large angular momentum regime, i.e., $l \gg 1$, we can recover (42). Again, this correspondence is usually accurate in the eikonal regime, but in some cases, it is also accurate even for small multipole number l . To verify this, we use the shadow radius expressed in (39) in order to compute the real part of QNMs frequencies from (45). In Table IV, we present numerical results of the shadow radius and the real part of QNMs frequencies for a given multipole number l by varying the magnitude of electric charge q_e . When we compare the numerical results presented in Table IV with the results obtained using the WKB method for the scalar (Table I) and electromagnetic field perturbations (II and III), we see that for small l , the accuracy and precision between two methods is higher for the scalar field perturbations. In the case of electromagnetic field perturbations, we observe a higher accuracy for modes I in comparison to modes II. Indeed, the accuracy and precision of the above two methods increase with the multipole number l .

TABLE IV. Numerical values of the shadow radius and the real part of QNMs frequencies obtained via (45).

	$l = 1, n = 0$	$l = 2, n = 0$	$l = 3, n = 0$	$l = 4, n = 0$	
q_e	ω_{\Re}	ω_{\Re}	ω_{\Re}	ω_{\Re}	R_s
0	1.0	1.5	2.0	2.5	2.0
0.1	1.000235918	1.500353876	2.000471835	2.500589794	1.999528276
0.2	1.001899545	1.502849318	2.003799091	2.504748864	1.996208112
0.3	1.006526831	1.509790247	2.013053662	2.516317078	1.987030984
0.4	1.016051116	1.524076674	2.032102232	2.540127790	1.968404905
0.5	1.033537114	1.550305671	2.067074228	2.583842785	1.935102255

VI. ABSORPTION CROSS-SECTION

In this section, we are going to determine the partial absorption cross-section in 5D electrically charged Bardeen black holes spacetime. This is another important quantity which in D-dimensions can be defined as following [85]:

$$\sigma_l = \frac{\pi^{\frac{D-2}{2}}}{\Gamma(\frac{D-2}{2}) \omega^{D-2}} \frac{(l+D-4)!(2l+D-3)}{l!} |T_l(\omega)|^2. \quad (46)$$

Thus, in case of the 5D electrically charged Bardeen spacetime, the partial absorption cross-section reads simply

$$\sigma_l = \frac{4\pi(l+1)^2}{\omega^3} |T_l(\omega)|^2. \quad (47)$$

Furthermore, it could be useful to define the total absorption cross-section, which can be given by

$$\sigma = \frac{\pi^{\frac{D-2}{2}}}{\Gamma(\frac{D-2}{2}) \omega^{D-2}} \sum_{l=0}^{\infty} \frac{(l+D-4)!(2l+D-3)}{l!} |T_l(\omega)|^2. \quad (48)$$

In Figs. 13 and 14, we plot the partial absorption cross-section versus ω for the scalar and electromagnetic field perturbations, respectively. From these plots, we can see that the partial absorption cross-section decreases by increasing the magnitude of the electric charge q_e . In particular, for a given value of the electric charge q_e , we see that the partial absorption cross-section initially increases with an increasing value of ω . It reaches the maximum value at some critical value of ω . Then it decreases in the limit of large ω since the partial absorption cross-section behaves like the inverse of ω^3 .

In high energy scale regime, the wavelength is considered to be negligible relative to the horizon scale of the black hole. Hence, one could identify the classical capture cross-section of the light

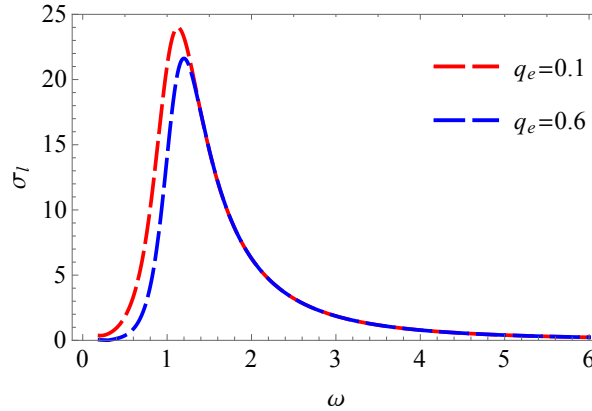


FIG. 13. The plot shows the dependence of partial absorption cross-section versus frequency of the scalar field perturbations ($\mu = 1$ and $l = 1$).

rays with the geometric cross-section of the light rays given by the the expression [85, 86]

$$\sigma_{geom} = \frac{\pi^{\frac{D-2}{2}} b_{ps}^{D-2}}{\Gamma(D/2)}, \quad (49)$$

where b_{ps} is the critical impact parameter of the light rays. It can be defined as the ratio of the angular momentum and the photon's energy moving along the spherical photon orbits, i.e., $b_{ps} = J/E$. Now we can use the geometric-optics correspondence between the parameters of the QNMs frequencies and the conserved quantities along geodesics. In particular, the particle energy can be identified as the real part of the QNMs frequencies. Besides, the azimuthal quantum number corresponds to the angular momentum [87], hence, we can quickly express

$$E \rightarrow \omega_{\Re}, \quad \text{and} \quad J \rightarrow l. \quad (50)$$

It means that we can identify the impact parameter of the light rays with the shadow radius, i.e., $b_{ps} \rightarrow R_s$. Further, we can use (42) to express the geometric cross-section in terms of the real part of the QNMs frequency as follows

$$\sigma_{geom} = \lim_{l \gg 1} \frac{\pi^{\frac{D-2}{2}} l^{D-2}}{\Gamma(D/2) \omega_{\Re}^{D-2}}, \quad (51)$$

which is valid in the eikonal regime. As we have already pointed out that due to the symmetry of the scattering properties, the greybody factors are also present in the emission spectrum of the black holes. In other words, if the black hole emits in the eikonal regime, the same connection between the real part of the QNMs frequency and the geometric cross-section given by (51) is to be expected. Basically, this means that one can calculate the geometric cross-section by using the

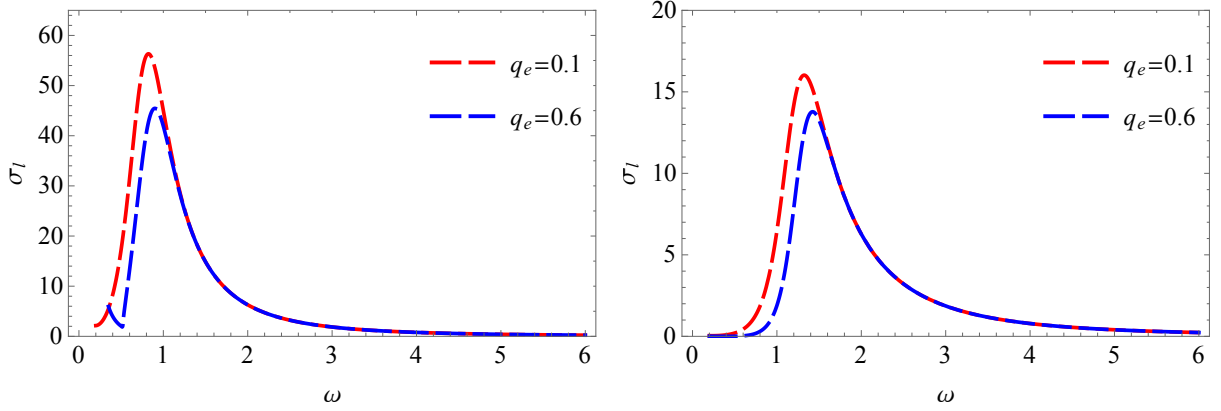


FIG. 14. (Left panel) Plot shows the dependence of partial absorption cross-section versus frequency in case of modes **I** of the electromagnetic field perturbations. (Right panel) Plot shows the dependence of partial absorption cross-section versus frequency in case of modes **II** of the electromagnetic field perturbations ($\mu = 1$ and $l = 1$).

real part of the QNMs frequencies. To the best of our knowledge, a relation between the geometric cross-section and the real part of the QNMs frequencies has not been explored before. Before we proceed to calculate the total absorption cross-section, let us point that in Ref. [85], it has been shown that there are fluctuations (of regular oscillations) of the high-energy (frequency) absorption cross-section around the limiting value of the geometric cross-section. In particular, it was found that the oscillatory part of the absorption cross-section of the massless scalar waves is given [85] by

$$\sigma_{osc} = (-1)^{D-3} 4(D-2)\pi\lambda R_s e^{-\pi\lambda R_s} \sigma_{geom} \text{sinc}(2\pi R_s \omega), \quad (52)$$

where we have used the correspondence, $b_{ps} \rightarrow R_s$. Moreover, the function has been introduced $\text{sinc}(x) = \sin(x)/x$ and λ is the Lyapunov exponent used for the analysis of the instability of the null geodesics. This means that the total absorption cross-section of the massless scalar waves is the sum of the geometric and the oscillatory cross-sections

$$\sigma \approx \sigma_{geom} + \sigma_{osc}. \quad (53)$$

From Eq. (51), we can easily find that in case of the 5D black holes, the geometric cross-section can be expressed in terms of the real part of the QNMs frequency as follows

$$\sigma_{geom} = \lim_{l \gg 1} \frac{4\pi l^3}{3\omega_{\mathfrak{R}}^3}. \quad (54)$$

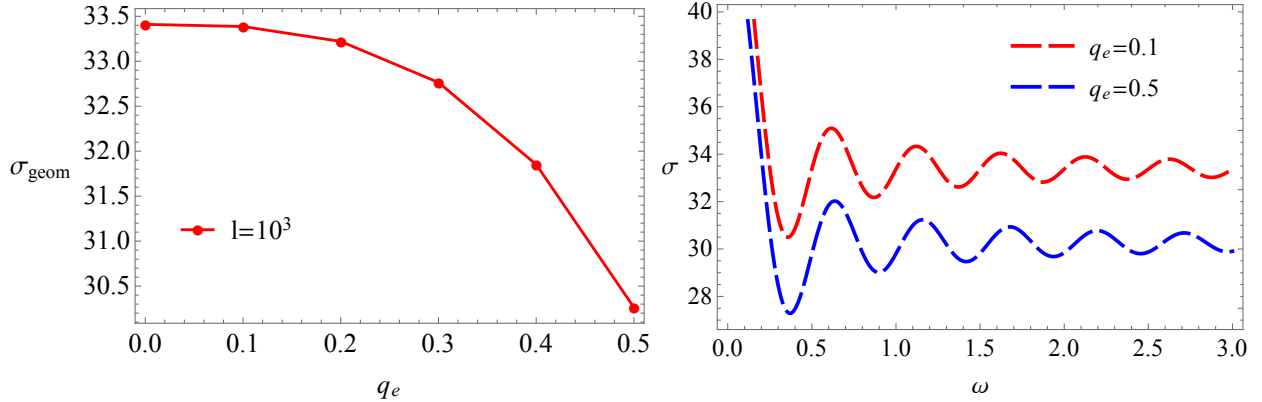


FIG. 15. (Left panel) Geometric cross-section as a function of electric charge q_e . In both plots we have used the scalar field perturbation to calculate $\omega_{\mathfrak{R}}$ with $\mu = 1$. One can reach the same conclusion using the electromagnetic field perturbations, provided $l \gg 1$. (Right panel) Plot of the total absorption cross-section versus frequency of the scalar field perturbations. We have used $q_e = 0.1$ (red curve) and $q_e = 0.5$ (blue curve), respectively ($l = 10^3$, $\lambda = 0.8$ and $\mu = 1$).

In Fig. 15 (left panel), we portrait the geometric cross-section as a function of the electric charge q_e . We see that the geometric cross-section decreases with an increase in the magnitude of the electric charge q_e . We find that in the eikonal limit, the geometric cross-section and the shadow radius share a similar behavior with respect to the electric charge q_e which can be explained from the fact that the geometric cross-section scales with the shadow radius. On the other hand, the oscillatory part in case of the 5D black holes reads simply

$$\sigma_{osc} = 12\pi\lambda R_s e^{-\pi\lambda R_s} \sigma_{geom} \text{sinc}(2\pi R_s \omega). \quad (55)$$

In Fig. 15 (right panel), we show the total absorption cross-section as a function of ω and fixed values of the electric charge q_e in case of the scalar field perturbations. We see that the total absorption cross-section decreases by increasing the electric charge q_e . In this sense, our result is consistent with effect of the electric charge in case of the 4D electrically charged black hole and generalizes the results reported in [85].

VII. CONCLUSION

In this work, we have performed a comprehensive discussion on QNMs in 5D electrically charged Bardeen black holes spacetime. The study has provided impressive results in five dimensions when considering general relativity coupled to the nonlinear electrodynamics. To compute the QNMs

frequencies, we have discussed the scalar and the electromagnetic field perturbations. We have used the WKB approach up to sixth order to determine the numerical values of the QNMs frequencies. The effect of nonlinear electric charge q_e on the QNMs frequencies has been investigated, which provides a significant impact. In studying the scalar field perturbations, it has been found that the electric charge q_e increases the real part of the QNMs frequencies and decreases the imaginary part of the QNMs frequencies in an absolute amount. While discussing the electromagnetic field perturbations, we discovered that an increase in the electric charge q_e increases the real part of the QNMs frequencies and decreases the imaginary part of the QNMs frequencies in absolute value in both cases of the modes **I** and **II**, respectively. We have noticed that the numerical values of the QNMs frequencies are higher in the scalar field perturbations compared to the electromagnetic field perturbations. This indicates that the scalar field perturbations oscillate more rapidly in comparison to the electromagnetic field perturbations. On the other hand, the scalar field perturbations damp more quickly than the electromagnetic field perturbations.

In further analysis, we have discussed the scattering and the greybody factors. We calculated analytical expressions of the reflection and the transmission coefficients. It has been found that the reflection coefficient increases with electric charge q_e while the transmission coefficient decreases with electric charge q_e . We extended our analysis to determine a direct connection between the black holes' shadows and the QNMs frequencies. The null geodesics and spherical photon orbits conditions have been discussed to describe the shadow of black holes. The black holes' shadows have been portrayed by varying electric charge q_e , and its typical behavior, has also been discussed. We have found that the presence of electric charge q_e affects the radius of the black hole shadow, which decreases by an increase in the magnitude of electric charge q_e . We have shown that this result can be obtained by means of the real part of the QNMs frequencies valid in the eikonal limit. We have also discussed how the electric charge q_e affects the partial absorption cross-section in case of 5D electrically charged black holes. Finally, we have explored the total absorption cross-section in the high energy scale, which consists of the geometric cross-section and oscillatory parts. Importantly, we have expressed the geometric cross-section in terms of the real part of the QNMs frequencies by using the geometric-optics correspondence. Our result shows that the total absorption cross-section decreases with an increase in the magnitude of electric charge q_e .

Our work can be extended to AdS spaces as they open a new avenue on the onset of the connection of the photon orbits to the thermodynamic phase transition of the AdS black holes. On the other hand, the black hole shadows and the QNMs frequencies of the AdS black holes are connected with the stability, the thermodynamic phase transition, and the hydrodynamic region

of strongly coupled field theories. Hence, the study of the QNMs in the 5D electrically charged regular AdS black holes and its connection to the shadow properties will be a natural extension of our work in a future project.

ACKNOWLEDGMENTS

MA acknowledges that this research work is supported by the National Research Foundation, South Africa. MSA's research is supported by the ISIRD grant 9-252/2016/IITRPR/708. SDM acknowledges that this work is based on research supported by the South African Research Chair Initiative of the Department of Science and Technology and the National Research Foundation. We are indebted to the anonymous referee for useful comments and suggestions.

-
- [1] S. Hawking and R. Penrose, *Proc. Roy. Soc. Lond. A* **A314**, 529 (1970).
 - [2] J. M. Bardeen, in *Proceedings of GR5* (Tiflis, U.S.S.R., 1968).
 - [3] V. P. Frolov, *Phys. Rev. D* **94**, 104056 (2016), arXiv:1609.01758 [gr-qc].
 - [4] E. Ayon-Beato and A. Garcia, *Phys. Lett. B* **493**, 149 (2000), arXiv:gr-qc/0009077.
 - [5] E. Ayon-Beato and A. Garcia, *Phys. Rev. Lett.* **80**, 5056 (1998), arXiv:gr-qc/9911046.
 - [6] E. Ayon-Beato and A. Garcia, *Phys. Lett. B* **464**, 25 (1999), arXiv:hep-th/9911174.
 - [7] E. Ayon-Beato and A. Garcia, *Gen. Rel. Grav.* **31**, 629 (1999), arXiv:gr-qc/9911084.
 - [8] I. Dymnikova, *Int. J. Mod. Phys. D* **12**, 1015 (2003), arXiv:gr-qc/0304110.
 - [9] M. R. Mbonye and D. Kazanas, *Phys. Rev. D* **72**, 024016 (2005), arXiv:gr-qc/0506111.
 - [10] S. A. Hayward, *Phys. Rev. Lett.* **96**, 031103 (2006), arXiv:gr-qc/0506126.
 - [11] C. Bambi, *Mod. Phys. Lett. A* **26**, 2453 (2011), arXiv:1109.4256 [gr-qc].
 - [12] C. Bambi, *Astron. Rev.* **8**, 4 (2013), arXiv:1301.0361 [gr-qc].
 - [13] M. S. Ali and S. G. Ghosh, (2019), arXiv:1906.11284 [gr-qc].
 - [14] A. Abdujabbarov, M. Amir, B. Ahmedov, and S. G. Ghosh, *Phys. Rev. D* **93**, 104004 (2016), arXiv:1604.03809 [gr-qc].
 - [15] M. Amir and S. G. Ghosh, *Phys. Rev. D* **94**, 024054 (2016), arXiv:1603.06382 [gr-qc].
 - [16] S. G. Ghosh, P. Sheoran, and M. Amir, *Phys. Rev. D* **90**, 103006 (2014), arXiv:1410.5588 [gr-qc].
 - [17] M. Amir and S. G. Ghosh, *JHEP* **07**, 015 (2015), arXiv:1503.08553 [gr-qc].
 - [18] S. G. Ghosh and M. Amir, *Eur. Phys. J. C* **75**, 553 (2015), arXiv:1506.04382 [gr-qc].
 - [19] C. Bambi, L. Modesto, and L. Rachwał, *JCAP* **05**, 003 (2017), arXiv:1611.00865 [gr-qc].
 - [20] S. G. Ghosh, D. V. Singh, and S. D. Maharaj, *Phys. Rev. D* **97**, 104050 (2018).
 - [21] A. Kumar, D. Veer Singh, and S. G. Ghosh, *Eur. Phys. J. C* **79**, 275 (2019), arXiv:1808.06498 [gr-qc].

- [22] C. H. Nam, *Gen. Rel. Grav.* **51**, 100 (2019).
- [23] S. Hyun and C. H. Nam, *Eur. Phys. J. C* **79**, 737 (2019), [arXiv:1908.09294 \[gr-qc\]](#).
- [24] R. Aros and M. Estrada, *Eur. Phys. J. C* **79**, 259 (2019), [arXiv:1901.08724 \[gr-qc\]](#).
- [25] M. Ali and S. G. Ghosh, *Phys. Rev. D* **98**, 084025 (2018).
- [26] T. Regge and J. A. Wheeler, *Phys. Rev.* **108**, 1063 (1957).
- [27] F. Zerilli, *Phys. Rev. D* **9**, 860 (1974).
- [28] C. Vishveshwara, *Phys. Rev. D* **1**, 2870 (1970).
- [29] C. Vishveshwara, *Nature* **227**, 936 (1970).
- [30] S. Chandrasekhar and S. L. Detweiler, *Proc. Roy. Soc. Lond. A* **A344**, 441 (1975).
- [31] R. Konoplya, *Phys. Rev. D* **71**, 024038 (2005), [arXiv:hep-th/0410057](#).
- [32] J. Natario and R. Schiappa, *Adv. Theor. Math. Phys.* **8**, 1001 (2004), [arXiv:hep-th/0411267](#).
- [33] A. Nagar and L. Rezzolla, *Class. Quant. Grav.* **22**, R167 (2005), [Erratum: *Class.Quant.Grav.* 23, 4297 (2006)], [arXiv:gr-qc/0502064](#).
- [34] R. Konoplya and A. Zhidenko, *Phys. Lett. B* **644**, 186 (2007), [arXiv:gr-qc/0605082](#).
- [35] G. Panotopoulos, *Axioms* **9**, 33 (2020), [arXiv:2005.08338 \[gr-qc\]](#).
- [36] V. Ferrari, M. Pauri, and F. Piazza, *Phys. Rev. D* **63**, 064009 (2001), [arXiv:gr-qc/0005125](#).
- [37] X.-Z. Li, J.-G. Hao, and D.-J. Liu, *Phys. Lett. B* **507**, 312 (2001), [arXiv:gr-qc/0205007](#).
- [38] B. Toshmatov, A. Abdujabbarov, Z. e. Stuchlk, and B. Ahmedov, *Phys. Rev. D* **91**, 083008 (2015), [arXiv:1503.05737 \[gr-qc\]](#).
- [39] G. Panotopoulos and . Rincn, *Eur. Phys. J. Plus* **134**, 300 (2019), [arXiv:1904.10847 \[gr-qc\]](#).
- [40] R. Konoplya, *Phys. Rev. D* **68**, 024018 (2003), [arXiv:gr-qc/0303052](#).
- [41] R. Konoplya and A. Zhidenko, *Rev. Mod. Phys.* **83**, 793 (2011), [arXiv:1102.4014 \[gr-qc\]](#).
- [42] M. Purrer, S. Husa, and P. C. Aichelburg, *Phys. Rev. D* **71**, 104005 (2005), [arXiv:gr-qc/0411078](#).
- [43] K. Akiyama *et al.* (Event Horizon Telescope), *Astrophys. J.* **875**, L1 (2019), [arXiv:1906.11238 \[astro-ph.GA\]](#).
- [44] K. Akiyama *et al.* (Event Horizon Telescope), *Astrophys. J. Lett.* **875**, L5 (2019), [arXiv:1906.11242 \[astro-ph.GA\]](#).
- [45] K. Akiyama *et al.* (Event Horizon Telescope), *Astrophys. J. Lett.* **875**, L6 (2019), [arXiv:1906.11243 \[astro-ph.GA\]](#).
- [46] M. Amir, A. Banerjee, and S. D. Maharaj, *Annals Phys.* **400**, 198 (2019), [arXiv:1805.12435 \[gr-qc\]](#).
- [47] M. Amir, K. Jusufi, A. Banerjee, and S. Hansraj, *Class. Quant. Grav.* **36**, 215007 (2019), [arXiv:1806.07782 \[gr-qc\]](#).
- [48] K. Jusufi, M. Jamil, P. Salucci, T. Zhu, and S. Haroon, *Phys. Rev. D* **100**, 044012 (2019), [arXiv:1905.11803 \[physics.gen-ph\]](#).
- [49] K. Jusufi, M. Jamil, and T. Zhu, *Eur. Phys. J. C* **80**, 354 (2020), [arXiv:2005.05299 \[gr-qc\]](#).
- [50] S. Haroon, K. Jusufi, and M. Jamil, *Universe* **6**, 23 (2020), [arXiv:1904.00711 \[gr-qc\]](#).

- [51] S. Vagnozzi, C. Bambi, and L. Visinelli, *Class. Quant. Grav.* **37**, 087001 (2020), [arXiv:2001.02986 \[gr-qc\]](#).
- [52] A. Allahyari, M. Khodadi, S. Vagnozzi, and D. F. Mota, *JCAP* **02**, 003 (2020), [arXiv:1912.08231 \[gr-qc\]](#).
- [53] S. Vagnozzi and L. Visinelli, *Phys. Rev. D* **100**, 024020 (2019), [arXiv:1905.12421 \[gr-qc\]](#).
- [54] C. Bambi, K. Freese, S. Vagnozzi, and L. Visinelli, *Phys. Rev. D* **100**, 044057 (2019), [arXiv:1904.12983 \[gr-qc\]](#).
- [55] M. Khodadi, A. Allahyari, S. Vagnozzi, and D. F. Mota, (2020), [arXiv:2005.05992 \[gr-qc\]](#).
- [56] A. Narang, S. Mohanty, and A. Kumar, (2020), [arXiv:2002.12786 \[gr-qc\]](#).
- [57] B. Abbott *et al.* (LIGO Scientific, Virgo), *Phys. Rev. Lett.* **116**, 061102 (2016), [arXiv:1602.03837 \[gr-qc\]](#).
- [58] . Rincn and G. Panotopoulos, *Eur. Phys. J. C* **78**, 858 (2018), [arXiv:1810.08822 \[gr-qc\]](#).
- [59] P. Kanti and J. March-Russell, *Phys. Rev. D* **66**, 024023 (2002), [arXiv:hep-ph/0203223](#).
- [60] M. Amir, M. S. Ali, and S. D. Maharaj, (2020), [arXiv:2005.00307 \[gr-qc\]](#).
- [61] K. Jusufi, *Phys. Rev. D* **101**, 084055 (2020), [arXiv:1912.13320 \[gr-qc\]](#).
- [62] B. Cuadros-Melgar, R. Fontana, and J. de Oliveira, (2020), [arXiv:2005.09761 \[gr-qc\]](#).
- [63] K. Jusufi, *Phys. Rev. D* **101**, 124063 (2020), [arXiv:2004.04664 \[gr-qc\]](#).
- [64] K. A. Bronnikov, *Phys. Rev. D* **63**, 044005 (2001), [arXiv:gr-qc/0006014](#).
- [65] K. Bronnikov, V. Melnikov, and H. Dehnen, *Gen. Rel. Grav.* **39**, 973 (2007), [arXiv:gr-qc/0611022](#).
- [66] K. A. Bronnikov, *Phys. Rev. D* **96**, 128501 (2017), [arXiv:1712.04342 \[gr-qc\]](#).
- [67] K. Bronnikov, V. Melnikov, G. Shikin, and K. Staniukowicz, *Annals Phys.* **118**, 84 (1979).
- [68] B. F. Schutz and C. M. Will, *The Astrophysical Journal* **291**, L33 (1985).
- [69] E. Leaver, *Proc. Roy. Soc. Lond. A* **A402**, 285 (1985).
- [70] H.-J. Blome and B. Mashhoon, *Physics Letters A* **100**, 231 (1984).
- [71] V. Ferrari and B. Mashhoon, *Phys. Rev. D* **30**, 295 (1984).
- [72] S. Iyer and C. M. Will, *Physical Review D* **35**, 3621 (1987).
- [73] L. D. Landau and E. M. Lifshitz, *The Classical Theory of Fields*, Course of Theoretical Physics Series (Butterworth-Heinemann, Oxford, 1987), Vol. 2, 4th ed..
- [74] C. Molina, *Phys. Rev. D* **68**, 064007 (2003), [arXiv:gr-qc/0304053](#).
- [75] R. Konoplya, Z. Stuchlk, and A. Zhidenko, *Phys. Rev. D* **98**, 104033 (2018), [arXiv:1808.03346 \[gr-qc\]](#).
- [76] L. C. Crispino, A. Higuchi, and G. E. Matsas, *Phys. Rev. D* **63**, 124008 (2001), [Erratum: *Phys.Rev.D* **80**, 029906 (2009)], [arXiv:gr-qc/0011070](#).
- [77] A. Lopez-Ortega, *Gen. Rel. Grav.* **38**, 1747 (2006), [arXiv:gr-qc/0605034](#).
- [78] H. Kodama and A. Ishibashi, *Prog. Theor. Phys.* **111**, 29 (2004), [arXiv:0308128 \[hep-th\]](#).
- [79] M. Amir, B. P. Singh, and S. G. Ghosh, *Eur. Phys. J. C* **78**, 399 (2018), [arXiv:1707.09521 \[gr-qc\]](#).
- [80] T. Johannsen, *Astrophys. J.* **777**, 170 (2013), [arXiv:1501.02814 \[astro-ph.HE\]](#).

- [81] V. Cardoso, A. S. Miranda, E. Berti, H. Witek, and V. T. Zanchin, *Phys. Rev. D* **79**, 064016 (2009), [arXiv:0812.1806 \[hep-th\]](#).
- [82] I. Z. Stefanov, S. S. Yazadjiev, and G. G. Gyulchev, *Phys. Rev. Lett.* **104**, 251103 (2010), [arXiv:1003.1609 \[gr-qc\]](#).
- [83] C. Liu, T. Zhu, Q. Wu, K. Jusufi, M. Jamil, M. Azreg-Anou, and A. Wang, *Phys. Rev. D* **101**, 084001 (2020), [arXiv:2003.00477 \[gr-qc\]](#).
- [84] R. Konoplya and Z. Stuchlk, *Phys. Lett. B* **771**, 597 (2017), [arXiv:1705.05928 \[gr-qc\]](#).
- [85] Y. Decanini, G. Esposito-Farese, and A. Folacci, *Phys. Rev. D* **83**, 044032 (2011), [arXiv:1101.0781 \[gr-qc\]](#).
- [86] B. Toshmatov, Z. e. Stuchlk, J. Schee, and B. Ahmedov, *Phys. Rev. D* **93**, 124017 (2016), [arXiv:1605.02058 \[gr-qc\]](#).
- [87] H. Yang *et al.*, *Phys. Rev. D* **86**, 104006 (2012), [arXiv:1207.4253 \[gr-qc\]](#).